Proceedings of the ASME Turbo Expo 2022
Turbomachinery Technical Conference and Exposition
GT2022
June 13-17, 2022, Rotterdam, The Netherlands

GT2022-83436

EVALUATION OF ADJOINT OPTIMIZED HOLES - PART I BASELINE PERFORMANCE

Daniel Gutierrez[1,*], Christopher Yoon[1], Michael T. Furgeson[1], Emma M. Veley[2], David G. Bogard[1], Karen A. Thole[2]

[1]The University of Texas at Austin
Austin, TX
[2]Pennsylvania State University
State College, PA

ABSTRACT

With the advent of the use of additive manufacturing to build gas turbine components, the design space for new hole geometries is essentially unlimited. Recently, a computational adjoint based optimization method was used to design shaped film cooling holes fed by internal co-flow and cross-flow channels. The associated RANS computations predicted that the holes optimized for use with cross-flow (X-AOpt) and co-flow (Co-AOpt) would significantly increase adiabatic effectiveness. However, only the X-AOpt hole was tested experimentally in this previous study. Though the experimentally measured performance for this hole was much less than computationally predicted, it still had a 75% improved performance compared to the conventional 7-7-7 shaped hole. In the current study, the X-AOpt and Co-AOpt shaped holes were experimentally evaluated using measurements of adiabatic effectiveness and overall cooling effectiveness. Coolant was fed to the holes with an internal co-flow channel. For reference, experiments were also conducted with the baseline 7-7-7 shaped hole, and a 15-15-1 shaped hole (shown in a previous study to be the optimum expansion angles for a shaped hole). Furthermore, overall cooling effectiveness measurements were made with engine scale models to evaluate the performance of additively manufactured (AM) X-AOpt and Co-AOpt holes with a realistic metal build. Results from this study confirmed that the X-AOpt hole had a 75% increase in adiabatic effectiveness compared to the 7-7-7 shaped hole. However, the Co-AOpt hole had only a 30% increase in adiabatic effectiveness, substantially less than had been computationally predicted. Measurements of overall cooling effectiveness for the engine-scale models and the large-scale models followed similar trends.

Keywords: film cooling, shaped holes, internal cooling, adjoint optimization, additive manufacturing

*Corresponding author: danielg7@utexas.edu

NOMENCLATURE

A_c	cross-sectional area [mm^2]
AM	additively manufactured
AOpt	adjoint optimized
D	metering hole diameter [m]
H	coolant channel height [m]
h	heat transfer coefficient [W/m^2-K]
k	thermal conductivity [W/m-K]
L	hole length [m]
P	pitch
RI	Rounded Inlet
SI	Sharp Inlet
T	temperature [K]
U	velocity [m/s]
X	downstream distance from hole [m]
Greek letters	
α	film cooling hole injection angle [°]
δ	uncertainty
η	adiabatic effectiveness
γ	specific heat ratio
ν	kinematic viscosity [m^2/s]
ϕ	overall effectiveness
ρ	density [kg/m^3]
Dimensionless groups	
Bi	Biot number, $h_\infty t/k_s$
C_d	discharge coefficient
DR	density ratio
M	blowing ratio
Ma	Mach Number
Pr	Prandtl number, ν/α
Re	Reynolds number, $U_\infty D/\nu$
VR	jet velocity ratio
VR_c	channel velocity ratio
Superscripts and subscripts	
∞	freestream condition

aw	adiabatic wall
b	bias
c	coolant
e	exit
f	fluid
h	hydraulic diameter
i	inlet
j	jet
p	precision
r	repeatability
s	solid
t	total

1. INTRODUCTION

This paper describes an experimental program to evaluate significantly improved film cooling configurations for cooling of gas turbine components. In recent years there have been many studies of radically new film cooling configurations that have been enabled by the flexibility of additive manufacturing and designed with various optimization processes. In this study, several advanced film cooling configurations, designed previously in our lab, were evaluated using measurements of adiabatic effectiveness and overall cooling effectiveness. Details of these new designs are presented below, followed by descriptions of the experimental program used in this study and the results of the experimental evaluation of performance.

In recent years, the viability of using additive manufacturing (AM) to manufacture turbine engine components has been established in several studies [1–5]. Schurb et al. [1] describe the evaluation by GE Power of the use of the AM process known as Selective Laser Melting (SLM) for manufacturing and repair of hot gas path parts for heavy duty gas turbine engines. They note the potential of this technique to become "a game changer for the production of future high performance, hot gas path parts". Min et al. [2] describe a metal AM build of a laidback fanshaped hole with a 1 mm metering hole diameter (defined as the diameter of a circular hole with the same cross-sectional area as the film cooling hole) using selective laser metal sintering (SLMS) processes. However, no quantification of the quality of the build of the holes was provided. Stimpson et al. [3] and Snyder and Thole [4] describe the use of laser powder bed fusion (L-PBF) processes for metal AM builds of 7-7-7 laidback fanshaped holes. Test coupons constructed for these studies incorporated film cooling holes made at engine scale with metering hole diameters as small 0.38 mm. These papers describe various construction methodologies that were studied to maximize the quality of the AM builds, and quantification of the roughness within the film cooling holes for the various build methods. Furthermore, the film cooling performance for various metal AM builds was evaluated using measurements of overall cooling effectiveness at operating conditions similar to engine conditions. Using a conventional electrical discharge machining (EDM) constructed film cooling hole as a standard, degradation of film cooling performance due to roughness in the holes was quantified.

Taking advantage of the flexibility in the film cooling hole geometries possible with AM, there have been a number of studies of unique designs and optimized designs for film cooling holes. Snyder and Thole [5] experimentally tested five different film cooling hole geometries that have been proposed in previous studies, and which relied on metal AM to be practical. These hole geometries were constructed at engine scale and their overall cooling effectiveness was determined in a test facility that included an internal coolant channel that provided coolant to the film cooling holes in a co-flow configuration. This study showed that in most cases these holes could be built close to design intent, though the performance of some were impacted by roughness at the hole exit. Furthermore, this study identified the importance of convective cooling inside the holes on overall cooling effectiveness.

Since essentially all film cooling holes are designed with a sharp angle to the surface in order to enhance the capability of the coolant jet to remain attached to the surface, there is a sharp edge at the inlet of the film cooling hole. This sharp turn at the inlet to coolant hole inherently causes a large separation region just inside the hole, which is quite detrimental to the performance of the hole. With conventional manufacturing techniques nothing can be done to change the geometry of the hole inlet, but with AM the hole inlet can be changed at will. Studies by Fraas et al. [6] and Jones et al.[7] investigated shaped film cooling hole designs with rounded inlets with the intent to mitigate the effects of coolant feed into the film cooling holes from coolant channels oriented in a cross-flow direction. These studies found rounding of the hole inlet increased adiabatic effectiveness from 10% to 50% depending on the internal coolant channel velocity relative to the mainstream velocity. Jones et al. [8] conducted a computational and experimental study to determine the optimum expansion angles for a shaped hole fed with a rounded inlet to maximize adiabatic effectiveness. The optimum configuration was found to be lateral expansion angles of 15° with a forward expansion angle of 1°, which was designated as the 15-15-1 RI hole, and is one of the holes tested the current study.

Using the flexibility of geometric design afforded by AM, Jones et al. [8] used computational predictions incorporating adjoint based optimization to develop designs for shaped holes which maximized adiabatic effectiveness for coolant channels oriented in the cross-flow and co-flow directions. Computationally, the adjoint optimized cross-flow hole, designated X-AOpt, was predicted to increase maximum area averaged adiabatic effectiveness by as much as 150% compared to a reference 7-7-7 hole, and the adjoint optimized co-flow hole, designated Co-AOpt, was predicted to increase performance by as much as 200% compared to a reference 7-7-7 hole. However experimental measurements were only made with the X-AOpt, and with a plenum feed of coolant rather than with cross-flow channel. The experimental measurements of adiabatic effectiveness for the X-AOpt hole were much less than predicted computationally, but still about 80% larger than the 7-7-7 hole. The primary focus of the current study was a thorough experimental evaluation of the adiabatic effectiveness and overall cooling effectiveness performance for the X-AOpt and Co-AOpt holes.

Film cooling performance was quantified using measurements of adiabatic effectiveness, η, defined by:

$$\eta = \frac{T_\infty - T_{aw}}{T_\infty - T_c} \tag{1}$$

where T_∞ is the mainstream temperature, T_{aw} is the adiabatic wall temperature, and T_c is the average coolant temperature at the channel inlet. Measurements of overall cooling effectiveness, ϕ, were also made to determine the combined effects of film cooling, bore cooling within the film cooling hole, and internal cooling from the internal coolant channels. The overall cooling effectiveness is defined by:

$$\phi = \frac{T_\infty - T_w}{T_\infty - T_c} \tag{2}$$

where T_w is the temperature of conducting wall. Note that overall effectiveness measurements require matching engine conditions for the ratio of external and internal heat transfer coefficients, h_e/h_i, and Biot number, Bi [9].

The coolant jet flow rates are presented in terms of two parameters, the jet to mainstream velocity ratio, VR=V_j/V_∞, and the blowing ratio, M=$\rho_j V_j/\rho_\infty V_\infty$, where V is the velocity, ρ is the density, and subscript j denotes the film jet. For this study the focus will be on VR, as it has been shown to be the optimal scaling parameter with varying density ratio, DR [10, 11]. The coolant flow rate in the internal channel is quantified using the mean coolant channel velocity to the mainstream velocity ratio: VR_c=V_c/V_∞.

In this study, 5X engine-scale X-AOpt and Co-AOpt shaped holes were experimentally evaluated through measurements of adiabatic effectiveness and overall cooling effectiveness. Testing was done using an internal coolant channel oriented in the co-flow direction relative to the mainstream. For comparison, measurements were also made using a 7-7-7 SI shaped hole (as baseline performance) and a 15-15-1 RI shaped hole. Furthermore, for all hole configurations, measurements of discharge coefficients were made for varying VR. To evaluate performances at engine scale, metal AM builds of engine scale models (1X models) were made and tested. Overall cooling effectiveness measurements were made for the 1X models at nominally engine Mach numbers for the X-AOpt, Co-AOpt, and 15-15-1 RI holes. Results from the 1X and 5X models are compared.

2. TEST FACILITIES AND EXPERIMENTAL METHODS

This study involved experimental measurements of various film cooling hole geometries using low conductivity test coupons for measurements of adiabatic effectiveness and high conductivity (matched Biot number) coupons for overall cooling effectiveness measurements. All experiments used internal coolant channels oriented in the co-flow direction. Test coupons with 5X scale film cooling holes were tested in the University of Texas at Austin, Turbulence and Turbine Cooling Research Laboratory (TTCRL) low-speed wind tunnel facility and 1X scale metal AM built coupons were tested at Pennsylvania State University, Steady Thermal Aero Research Turbine (START) Laboratory. The closed-loop, low-speed wind tunnel facility at the University of Texas at Austin, is shown schematically in Fig. 1. This facility includes a secondary flow loop that provides coolant to the film cooling holes. Liquid nitrogen is passed through a heat exchanger to cool the coolant flow. For this study, all experiments were conducted with a coolant density ratio of DR=ρ_c/ρ_∞=1.20 at the exit of the film cooling holes. Coolant air was directed

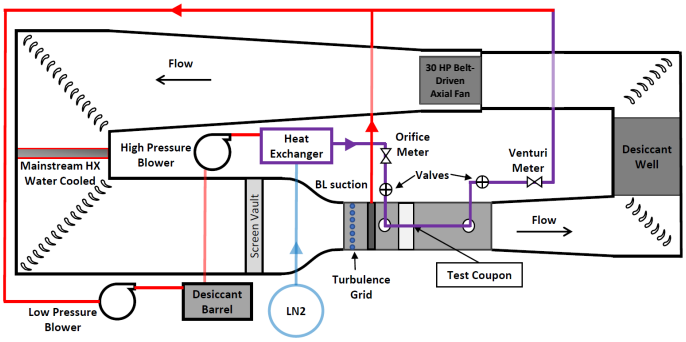

FIGURE 1: DIAGRAM OF WIND TUNNEL FACILITY USED FOR THE STUDY, TTCRL

through the test section coolant channel as shown in Fig. 2. The coolant channel was a rectangular channel with height H=3.4D and width W=74D with the flow in the channel directed in either a co-flow or counter-flow direction relative to the mainstream. For this study, all experiments were conducted using co-flow. The coolant temperatures at the inlet and outlet of the channel were measured using three type E thermocouples at each location noted on Fig. 2. To improve accuracy for thermocouple measurements, all thermocouples were calibrated using a high-accuracy thermistor in a constant temperature glycol bath. Static pressure taps installed in the channel floor were used to determine the inlet pressure for the coolant holes and the pressure drop across the length of the channel.

Measurements of the coolant flow rate entering and exiting the coolant channel were made using an orifice meter upstream of the inlet and a venturi meter downstream of the exit as shown in Fig. 1. The coolant mass flow rates for the film cooling holes were determined from the difference between the inlet and exit mass flow rates for the coolant feed channel. The test plate between the coolant channel and the mainstream includes a short film cooling hole coupon located 0.41 m downstream of the test plate leading edge. These film cooling hole coupons are 3D printed (described later) with various hole geometries and with low conductivity material for adiabatic effectiveness tests or high conductivity material for matched Bi tests. Downstream of the film cooling holes two different test plates were used, one with low conductivity material for adiabatic effectiveness tests and one with high conductivity material for matched Bi tests. The test plates were 3D in thickness. The low conductivity test plate was made with 1.5D layer of polyurethane foam with thermal conductivity of k≈0.03 W/m-K above a 1.5D layer of Corian used for structural strength. The high conductivity test plate was made with DuPont Corian with k≈1.0 W/m-K which yields a Biot number of Bi=0.89 for the mainstream velocity used in this study. An analysis performed by Dyson et al. estimated that the Biot number of an engine scale turbine airfoil ranges from Bi=0.1 to 1 [9]. This Biot number is representative of typical gas turbine engine operating conditions.

Overall effectiveness measurements for 1X scale models were performed using a START Laboratory facility with a test section shown schematically in Fig. 3. The mainstream channel in this facility had a hydraulic diameter of $D_{h,\infty}$=40D, where

D=0.76 mm was the design diameter for film cooling metering section. This facility also had a coolant channel with height H=3.4D, oriented for co-flow operation. This coolant channel was fed with gaseous nitrogen at the temperature needed to maintain a coolant density ratio of DR=1.2. The test coupons for this facility were AM built (described later) with Inconel 718, which resulted in a Biot number of Bi=0.15 for the operating conditions for this facility. Although this Biot number is significantly smaller than that for the 5X facility, it is within the range expected for engine operations. Furthermore, thermal analysis of the effect of this difference in Biot number showed that it would cause only a 4% increase in the overall cooling effectiveness. More information on details for the START Laboratory wind tunnel facility may be found in a recent study by Veley et al. [12].

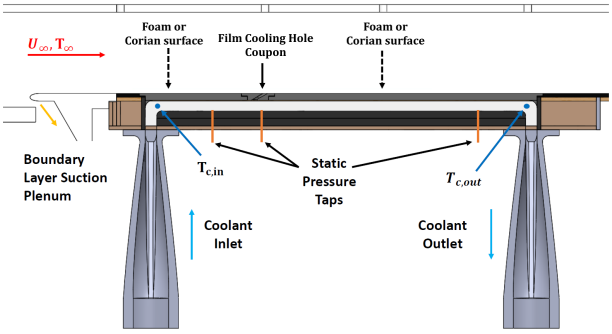

FIGURE 2: SCHEMATIC OF THE TEST SECTION, TTCRL

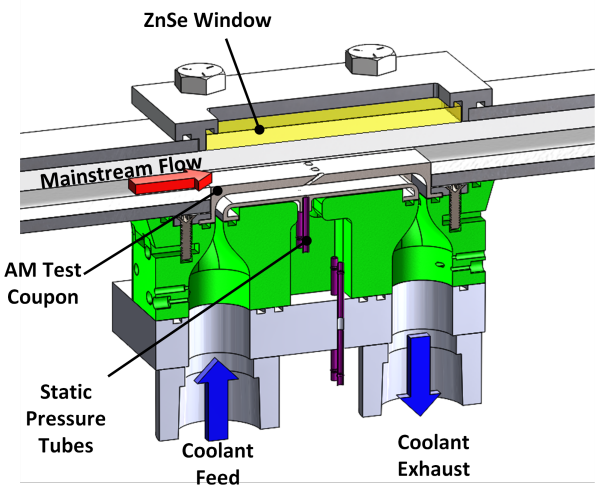

FIGURE 3: SCHEMATIC OF THE TEST SECTION, START LABORATORY

The film cooling hole geometries used in this analysis were laidback fanshaped holes. Geometries tested in this study were a baseline 7-7-7 SI shaped hole, 15-15-1 RI shaped hole, X-AOpt shaped hole, and Co-AOpt shaped hole. Geometric parameters for 15-15-1 RI and 7-7-7 SI holes may be found in Table 1. As noted in this table, the metering hole diameter for the 5X scale 15-15-1 RI and 7-7-7 SI holes was 3.8 mm. However, the metering hole diameters for the 5X scale X-AOpt and Co-AOpt hole geometries were 4.18 mm and 4.75 mm, respectively, i.e. 10% and 25% larger than the baseline hole diameter. It should be noted that the hole to hole pitch (P/D) for the X-AOpt and Co-AOpt holes is reduced to 5.45 and 4.8, respectively. To account for the differences in P/D for the four geometries tested, comparisons in performance were made by using superposition to estimate the performance at an equivalent P/D for all geometries. Superposition predicts that adiabatic effectiveness scales with the inverse of P/D. This analysis was verified in the experimental results of Gritsch et al. [19], for shaped holes with P/D>6. The adjustment of spatially averaged adiabatic effectiveness for an equivalent P/D=6 was made for all cooling performance results presented in this paper. Schematics of the X-AOpt and Co-AOpt holes are presented in Fig. 4. More details on these holes and the adjoint based optimization process used to design the holes are available in Jones et al. [13].

TABLE 1: HOLE GEOMETRY PARAMETERS FOR THE 7-7-7 SI, 15-15-1 RI, X-AOPT, AND CO-AOPT HOLES

Parameter	7-7-7 SI	15-15-1 RI	X-AOpt	Co-AOpt
Hole Diameter D (mm)	3.8	3.8	4.18	4.75
Hole Length L/D	6	6	5.45	4.8
Metering Hole Length L_m/D	2.5	2.5	2.27	2
Injection Angle α	30°	30°	30°	30°
Forward Expansion Angle β_{fwd}	7°	1°	[-]	[-]
Lateral Expansion Angle β_{lat}	7°	15°	[-]	[-]
Inlet Fillet Radius R/D	0.05	0.25	[-]	[-]
Hole-to-hole Pitch P/D	6	6	5.45	4.8

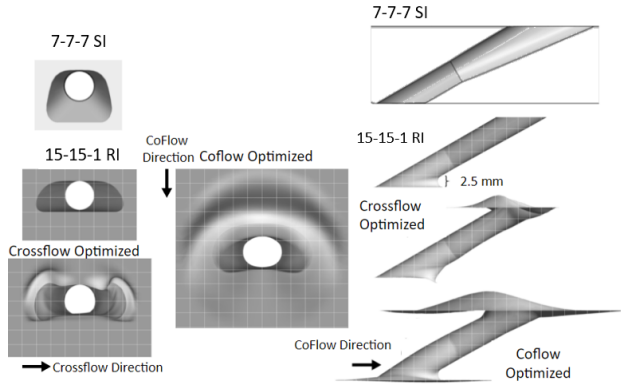

FIGURE 4: GEOMETRIES OF THE ADJOINT OPTIMIZED HOLES FOR CROSS-FLOW AND CO-FLOW ENTRY CONDITIONS. ALSO SHOWN ARE THE BASELINE 15-15-1 RI AND 7-7-7 SI SHAPED HOLES FOR REFERENCE.

Given the larger scale of the 5X models tested in this study, these models were built very close to the design geometry. However, the 1X scale metal AM models tested were as-built (AB), which deviated from the as-designed (AD) models used for the the 5X. Details of these deviations are presented in Furgeson et al. [14]. Using computer tomography (CT) scans, the deviations of the AB X-AOpt hole relative to the design intent was quantified as shown in Fig. 5. Reconstructions of the as-built surfaces of the holes were created using measurements from CT scans. From the surface determined from the CT scans, the minimum cross-sectional area, also known as the metering area, was determined.

Although the AB hole had the same general characteristics as the AD hole, the vertical height of the protrusions at the exit of the hole were reduced, and a lip formed at the center of the upstream edge of the hole. The metering area of every AB hole was larger by between 2-20% as compared to the design intent. The overall effectiveness measurements used the metering diameters for lateral and area averages of effectiveness. The 1X engine-scale hole geometries introduce surface roughness effects due to the nature of the print method. These AB geometries are rougher at the inlet and outlet of the hole, as well as the surface and differ slightly from the design intent AD models. In the aforementioned recent study by Ferguson et al., the differences in effectiveness due to roughness effects for the AB cases are explained in more detail and evaluated experimentally [14].

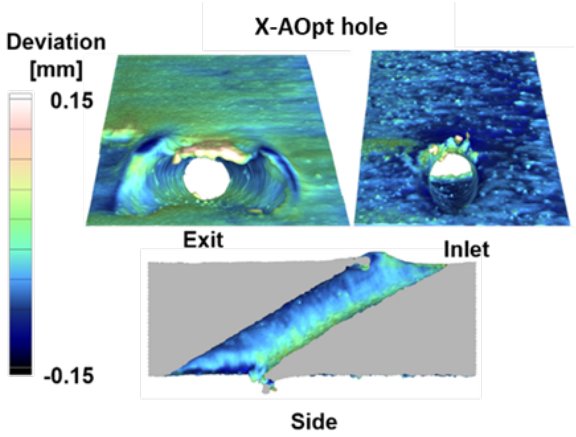

FIGURE 5: CT SCAN OF DEVIATIONS OF AB X-AOPT METAL COUPON

Low conductivity (adiabatic) and high conductivity (matched Bi) coupons containing film cooling shaped holes were built using additive manufacturing techniques. Fused Deposition Modeling (FDM) printers were used to build 5X scale coupons containing an array of 10 equally spaced film cooling holes. Infrared (IR) camera measurements were focused on the four holes at the center of the row of holes. The 5X scale low conductivity coupons were printed using Polylactic Acid (PLA) as filament while high conductivity coupons were printed using TCPoly, a conductive filament. The estimated thermal conductivity of this conductive nylon filament is $k \approx 1$ W/m-K in the surface-normal direction and $k \approx 4$ W/m-K in plane direction. More information on 5X engine-scale coupon printing methods may be found in a recent study by Furgeson et al. [14].

An EOS M 280 Direct Metal Laser Sintering (DMLS) printer was used to additively manufacture 1X engine-scale coupons at a 40 μm layer setting, using Inconel 718 (see Veley et al. [12] for details). Each of the three 1X engine-scale coupons tested had five engine-scale holes in the row of holes, with IR camera measurements focused on the center three holes. When being constructed, the coupons were oriented with the metering axis perpendicular to the substrate plate. Prior to the parts being taken off the substrate, internal stresses from the build process were removed through annealing the build plate. .

General experimental conditions for the 5X model tests are listed in Table 2. A series of experiments were conducted in which the inlet coolant channel velocity ratio was kept constant at VR_c=0.2 to evaluate performance for a constant given input coolant flow. Another series of experiments were done to simulate the operating conditions for the 1X model tests done with the START Laboratory facility. The operating conditions for the START facility are listed in Table 3. Besides the difference in scale for models tested in the two facilities, the mainstream Mach number for the START rig was Ma=0.3, which was substantially higher than the Ma=0.076 used in the TTCRL facility. As noted in Table 3, the tests conducted in the START facility maintained a constant coolant channel Reynolds number of Re_i=14,000 for the coolant channel downstream of the film cooling holes. However, when matching coolant channel Reynolds number in the large-scale facility, we found that the ratio of the external heat transfer coefficient to internal heat transfer coefficient, h_e/h_i, was not matched. Since matching the h_e/h_i ratio is critical for achieving similarity conditions to match the overall cooling effectiveness (see [10]), the coolant channel velocity was adjusted to obtain h_e/h_i=3.2, matching that for the high speed, small scale test facility. This required operating the coolant channel on the low speed, large scale facility at a channel velocity ratio of VR_c=0.12 downstream of the coolant holes, or a channel Reynolds number of Re_i=6,600.

TABLE 2: EXPERIMENTAL CONDITIONS, TTCRL

Parameter	Value	Units
Mainstream Velocity, U_∞	24.9	m/s
Mainstream Temperature, T_∞	295	K
Reynolds Number, Re_D	6200	[-]
Turbulence Intensity, Tu_∞	3.8	%
Boundary Layer Thickness, δ_{99}/D	2.5	[-]
Biot Number, Bi (Corian surface)	0.89	[-]
HTC Ratio, h_∞/h_c (Corian surface)	2.5	[-]
Density Ratio, DR	1.20	[-]
Velocity Ratio, VR	0.40 - 3.33	[-]

For the START facility, while the Reynolds number in the coolant supply channel was maintained at Re_i=14,000 downstream of the cooling holes, the upstream Reynolds number varied as coolant extracted from the channel through the film cooling holes varied with different blowing ratios. The reason for maintaining the downstream Reynolds number was to make sure the internal channel cooling did not vary downstream of the holes thereby providing a constant boundary condition for the overall effectiveness measurements. This method allowed for a direct comparison of the cooling holes and blowing ratios. The overall cooling effectiveness with no film cooling, ϕ_0, was measured with an internal channel Reynolds number of 14,000 and using a coupon with no cooling holes.

For the low speed, large scale facility, ϕ_0 was measured using a conductive coupon with no cooling holes, tested at various channel velocity ratios in the range of VR_c=0.1 to 0.4. As noted previously, to achieve similarity with 1X test conditions, the 5X facility needed to be operated with the same ratio of external to

internal heat transfer coefficients, i.e. h_e/h_i which was achieved by using an internal coolant channel velocity ratio of VR_c=0.12. Consequently, overall cooling effectiveness with no film cooling, ϕ_0, for the 5X facility was estimated for VR_c=0.12 downstream of the coolant holes using interpolation of the ϕ_0 measurements described previously. These measurements made it possible to examine the augmentation of cooling effectiveness, ϕ/ϕ_0, resulting solely from the film-cooling.

TABLE 3: EXPERIMENTAL CONDITIONS, START LABORATORY

Parameter	Coolant	Mainstream
Mach Number	<0.1	0.3
Upstream Re_i	Varied for M, D_h	
Downstream Re_i	14,000	
$Re_{D_h,\infty}$		220,000
Density Ratio,DR	1.23	

Surface temperature measurements for experiments conducted at the TTCRL facility were captured using an IR camera (FLIR A655SC), which was calibrated against surface thermocouples as described in Fox et al. [15]. The exterior surfaces of the Corian, foam, and FDM printed coupons were painted with a matte black paint to provide uniform surface emissivity. To maximize accuracy of temperature, pressure, and flow measurements, the associated instrumentation, i.e. thermocouples, pressure transducers, and orifice or venturi flow meters were carefully calibrated. In this process, the bias uncertainties for each of these instruments were estimated. Precision uncertainties were determined statistically from standard deviations for multiple repeated measurements. Uncertainties for discharge coefficients, adiabatic effectiveness, and overall cooling effectiveness were estimated using sequential perturbation methods as described by Moffat [16] to determine the propagation of uncertainties. The estimated bias and precision uncertainties for various measured variables are listed in Table 4. The total uncertainty for the adiabatic effectiveness was $\delta\eta$=±0.02 and for the overall cooling effectiveness $\delta\phi$=±0.02.

TABLE 4: MEAN BIAS AND PRECISION UNCERTAINTY

Parameter	$\pm\delta_p$	$\pm\delta_b$	Units
Mainstream Velocity, U_∞	0.1	0.01	m/s
Mainstream Temperature, T_∞	0.01	0.1	K
Coolant Temperature, T_c	0.1	0.1	K
Upstream Mass Flow Rate, $\dot{m}_o$	0.03	0.2	g/s
Downstream Mass Flow Rate, $\dot{m}_e$	0.04	0.2	g/s
Density Ratio, DR	0.0003	0.0007	[-]
Velocity Ratio, VR	0.01	0.1	[-]
Channel Inlet Velocity Ratio, VR_c	0.001	0.002	[-]
Overall Effectiveness, ϕ	0.001	0.02	[-]
Adiabatic Effectiveness, η	0.002	0.02	[-]

In all experiments conducted, the in-test repeatability of the measurements were checked by repeating measurements for a selected operating condition at the beginning and end of the experiment. Furthermore, test-to-test repeatability was checked by repeating a test of a selected test model in a second experiment done many days later. An example of test-to-test repeatability is shown in Fig. 6. For this example, a second experiment to measure adiabatic effectiveness for the X-AOpt hole was done after a five day span. As seen in Fig. 6, there was a shift in the measurement of $\bar{\eta}$ by about 0.01, which is well within the uncertainty estimate of $\bar{\eta}$=±0.02.

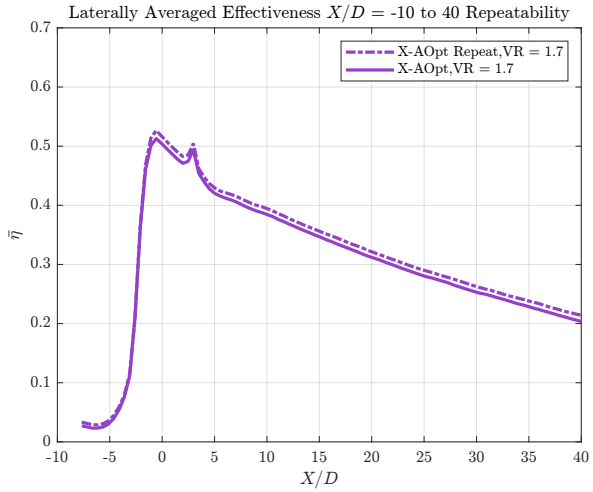

FIGURE 6: SAMPLE OF TEST-TO-TEST REPEATABILITY CHECK; LATERALLY-AVERAGED EFFECTIVENESS FOR THE X-AOPT HOLE AT *VR*=1.7

3. RESULTS

Discharge coefficients for all 5X engine-scale shaped hole models are presented, followed by the results of adiabatic and overall cooling effectiveness. For the top performing hole geometry, X-AOpt, further investigation of differences in hole-to-hole cooling effectiveness performance are reviewed. Overall cooling effectiveness results are also presented for the AM metal built 1X engine-scale 15-15-1 RI and X-AOpt shaped holes tested with engine representative high Mach number flows and compared to the results with the large scale, low speed wind tunnels tests.

3.1 Discharge Coefficient Measurements

Discharge coefficients for each hole as a function of VR were determined using measurements of the static pressure in the coolant channel at the inlet to the film cooling hole and the static pressure of the mainstream at the hole exit position, as well as the coolant temperature and the mass flow rate through the coolant holes. These measurements were made with the same low temperature coolant as used for the adiabatic and overall cooling effectiveness tests. The following equation, from Gritsch et al. [17], was used to determine C_d:

$$C_d = \frac{\dot{m}}{\frac{\pi d^2}{4} P_{t,c} \left(\frac{P_\infty}{P_{t,c}}\right)^{\frac{\gamma+1}{2\gamma}} \sqrt{\frac{2\gamma}{(\gamma-1)RT_{t,c}} \left(\left(\frac{P_{t,c}}{P_\infty}\right)^{\frac{\gamma-1}{\gamma}} - 1\right)}} \quad (3)$$

The discharge coefficient for the four holes studied in 5X adiabatic models are presented in Fig. 7. There was a noticeable variation in C_d values ranging from nominally C_d=0.8 for the 7-7-7 SI hole to C_d=1.2 for the X-AOpt hole. The 15-15-1 RI hole had C_d=0.9 at lower coolant jet *VR* values, which is similar to the C_d value reported by Gritsch et al. [18] for shaped holes which is similar in geometry to the 15-15-1 RI hole.

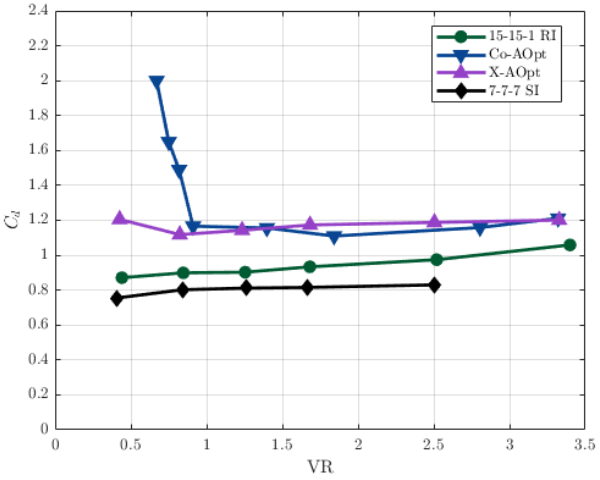

FIGURE 7: DISCHARGE COEFFICIENT MEASUREMENTS FOR ADIABATIC MODELS TESTED, *VRc*=0.20

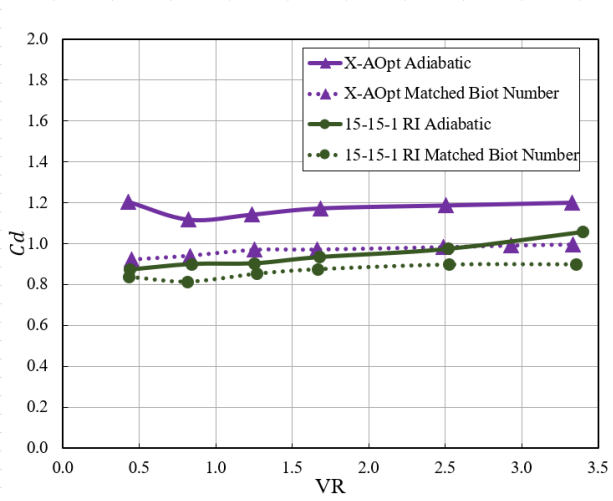

FIGURE 8: COMPARISON OF DISCHARGE COEFFICIENTS FOR THE ADIABATIC AND MATCHED *BI*) MODELS FOR THE X-AOPT AND 15-15-1 RI HOLES

As shown in Fig. 7, for the X-AOpt holes, $C_d \approx 1.2$, which is substantially higher than for the 15-15-1 RI and the 7-7-7 SI holes. Note that Gritsch et al.[17] found values of $C_d \approx 1.2$ for a laidback fanshaped hole at low pressure ratios for a co-flow fed hole. The increased C_d for the X-AOpt holes can be attributed to better pressure recovery in the diffuser section of the holes, and hence a decreased Δp from the inlet to the exit of the hole. A better recovery in the diffuser section of the X-AOpt hole compared to the 15-15-1 RI hole is consistent with computational study of Jones et al. [13] which showed a significant decrease in the coolant jet exit velocity for the X-AOpt hole compared to the 15-15-1 RI hole. Note that the definition used for defining C_d for film cooling holes, as represented by Eqn. 3, is based on the area of the throat of the film cooling hole, and does not account for the increase in area at the exit of the due to the diffuser section. Consequently, when the diffuser is designed to be more effective (less separation in the diffuser), the increase in pressure as the flow decelerates in the diffuser can lead to $C_d > 1$.

At *VR*=0.6, the Co-AOpt hole had a significant increase in discharge coefficient to $C_d \approx 2$. Repeated experiments in which the C_d was carefully measured several times confirmed that this was an accurate measurement. Furthermore, we found that this was largely due a decrease in static pressure at the hole exit caused by the sand dune shaped protrusion upstream of the hole exit.

Discharge coefficients were also measured for the matched *Bi* models for the 15-15-1 RI and X-AOpt holes, and results from these measurements are presented in Fig. 8 with comparisons to similar holes built in low conductivity coupons (for adiabatic effectiveness testing). Given that the same hole geometries were constructed in the low conductivity coupons and the high conductivity (matched *Bi*) coupons, one would expect similar C_d values. However, as is evident Fig. 8, the C_d values for the matched *Bi* coupons were lower than for the low conductivity models. For the X-AOpt hole the difference was significant, with the matched *Bi* model being 20% lower than the low conductivity model. For the 15-15-1 RI hole, the difference was only a slight difference with the matched *Bi* model being less than 10% lower than the low conductivity model.

These C_d results indicate that there were differences in the AM built hole geometries in the low and high conductivity coupons. This difference can be attributed to the different print methods used to build low and high conductivity coupons. As reported by Furgeson et al. [14], it has been shown that the conductive filament introduces surface roughness at the inlet and the outlet of the hole being printed. The X-AOpt low conductivity coupon is also printed with a finer layer height, which reduces surface roughness effects at the inlet and outlet of the hole.

3.2 Adiabatic Cooling Effectiveness Results

An overview of the adiabatic effectiveness results is presented in Fig. 9 for the four 5X holes tested. For this analysis, the area averaged adiabatic effectiveness was calculated over four hole pitches in the measurement range, and over the range *X/D*=5 to 20. As mentioned, adjustments of adiabatic film cooling effectiveness, $\bar{\bar{\eta}}$, were made for the X-AOpt and Co-AOpt hole geometries to match an equivalent *P/D*=6, i.e. the X-AOpt hole with *P/D*=5.45 is expected to have $(5.45/6)\bar{\bar{\eta}}_{meas}=0.91\bar{\bar{\eta}}_{meas}$ by superposition. The region of interest, *X/D*=5 to 20, was selected by Jones et al. [8] and [13] to develop the optimum hole geometries for the 15-15-1 RI and X-AOpt holes, respectively. Although somewhat arbitrary, the *X/D*=5 to 20 range was chosen to exclude the expected high effectiveness values in the near hole region so that this was not strongly weighted in the optimization process. The downstream distance of *X/D*=20 was chosen to cover a distance where the adiabatic effectiveness levels typically decrease

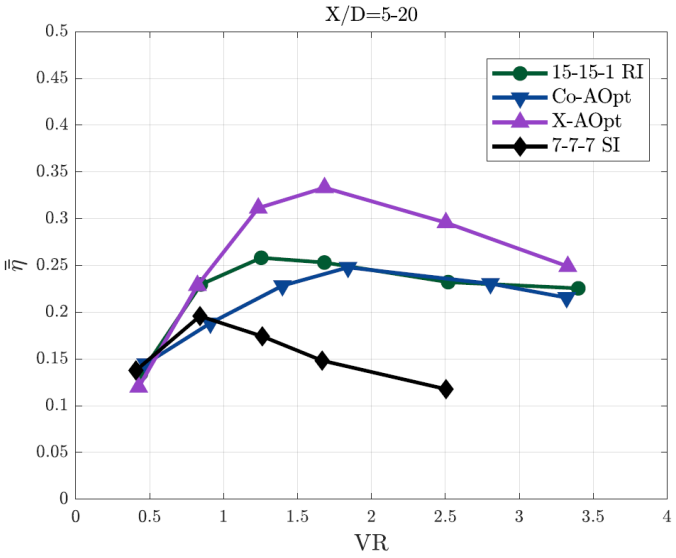

FIGURE 9: COMPARISON OF THE AREA AVERAGED ADIABATIC EFFECTIVENESS (*X/D*=5 TO 20) FOR THE X-AOPT, CO-AOPT, 15-15-1 RI, AND 7-7-7 SI HOLES. RESULTS ARE FOR AN EQUIVALENT *P/D*=6.

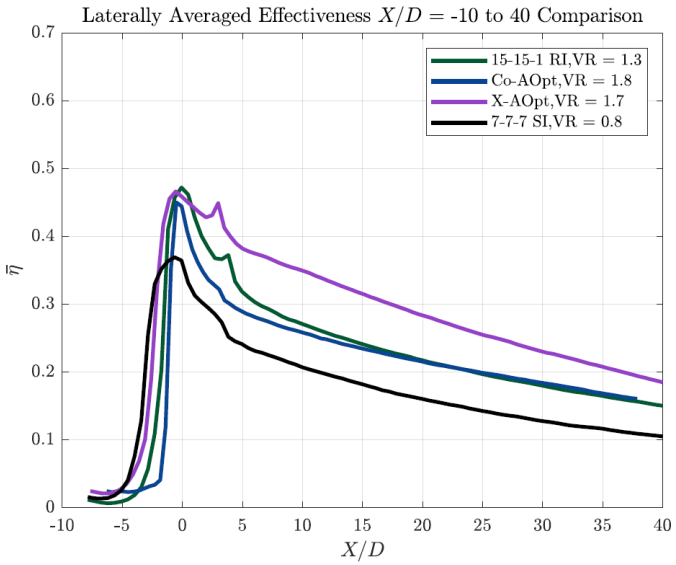

FIGURE 10: COMPARISON OF THE LATERALLY AVERAGED ADIABATIC EFFECTIVENESS FOR THE X-AOPT, CO-AOPT, 15-15-1 RI, AND 7-7-7 SI HOLES AT OPTIMUM *VR*c

by about 50%. As noted previously, the 7-7-7 SI was tested to provide a reference since this hole has been used extensively in past studies. The 15-15-1 RI hole that was found to have the optimum lateral and forward expansion angles in the study by Jones et al. [8]. The peak spatially averaged value for adiabatic effectiveness for the 15-15-1 RI hole was found to be $\bar{\bar{\eta}}$=0.26 at *VR*=1.3, which is consistent with the peak value found in the experiments by Jones et al. [8]. This peak value for $\bar{\bar{\eta}}$ for the 15-15-1 RI hole is 30% larger than the peak $\bar{\bar{\eta}}$ value for the 7-7-7 SI reference hole. Also evident in Fig. 9 is the significantly larger adiabatic effectiveness performance of the Co-AOpt and X-AOpt holes compared to the 7-7-7 SI hole. The Co-AOpt had a peak adiabatic effectiveness of $\bar{\bar{\eta}}$=0.25 and the X-AOpt had a peak adiabatic effectiveness of $\bar{\bar{\eta}}$=0.33, which are 30% and 75% larger than the reference 7-7-7 SI hole, respectively.

The peak adiabatic effectiveness measured for the X-AOpt hole was the same as that measured by Jones et al. [7], who designed the Co-AOpt and X-AOpt holes using an adjoint based optimization process. However, the coolant supply used in this previous study was a plenum feed in contrast to the co-flow coolant channel used in this study. Although Jones et al. [7] designed the Co-AOpt and X-AOpt holes, and computationally predicted their adiabatic effectiveness performance, they did not conduct experimental measurements to confirm the performance of the Co-AOpt hole. Their computational simulations predicted that the Co-AOpt hole would have significantly greater adiabatic effectiveness than the X-AOpt hole. The results shown in Fig. 9 are the first experimental comparisons of the performances of the Co-AOpt and X-AOpt. In contrast to the computational predictions, these experimental results show that the X-AOpt hole has significantly better performance than the Co-AOpt hole.

To provide more insight into adiabatic effectiveness performance for each of the four film cooling holes tested, the laterally averaged adiabatic effectiveness distributions, $\bar{\eta}$, are presented in Fig. 10 and contours of adiabatic effectiveness, η , are presented in Fig. 11. The $\bar{\eta}$ distributions shown in Fig. 10 show similar trends for all holes, but with distinctly higher $\bar{\eta}$ levels for the X-AOpt hole, and the lowest level for the reference 7-7-7 SI hole. Note that the anomalous spike for the 15-15-1 RI and X-AOpt holes at *X/D*=4 is an artifact due to a small gap between the film cooling hole coupon and the downstream test plate. This figure also shows that higher decay rates with downstream distance for the X-AOpt hole results in the $\bar{\eta}$ levels for this hole being only slightly higher than that for the 15-15-1 RI hole at *X/D*=40. However, the $\bar{\eta}$ levels for these three optimized holes are still a factor of 2 greater than $\bar{\eta}$ for the reference 7-7-7 hole at *X/D*=40.

As discussed in an earlier section, IR camera surface temperature measurements focused on four holes are presented as contours of η as shown by Fig 11. The width of the region of interest for all surface temperature measurements taken is four hole pitches using a reference diameter of 3.8 mm, up to 24D in width with a length up to 50D downstream of the film cooling holes (for the 7-7-7 SI and 15-15-1 RI geometries). Note that as the metering hole diameters for the X-AOpt and Co-AOpt are larger than the reference diameter, the *X/D* and Z/D ranges decrease slightly for those cases, but the length of the distance downstream, X, and width, Z, for the region of interest remains unchanged.

Significant differences in η distributions for the four holes at *VR* levels for maximum adiabatic effectiveness are evident in Fig. 11. Each of the optimized holes had much broader lateral spread of η than the reference 7-7-7 SI hole. The four holes in the row shown for 7-7-7 SI and 15-15-1 RI holes had essentially the same performance from each hole, flowed directly downstream with no skewness to one side or the other. In contrast to this, the four holes in the row shown for the Co-AOpt and X-AOpt holes had significant variation among the holes, and the exit of the coolant

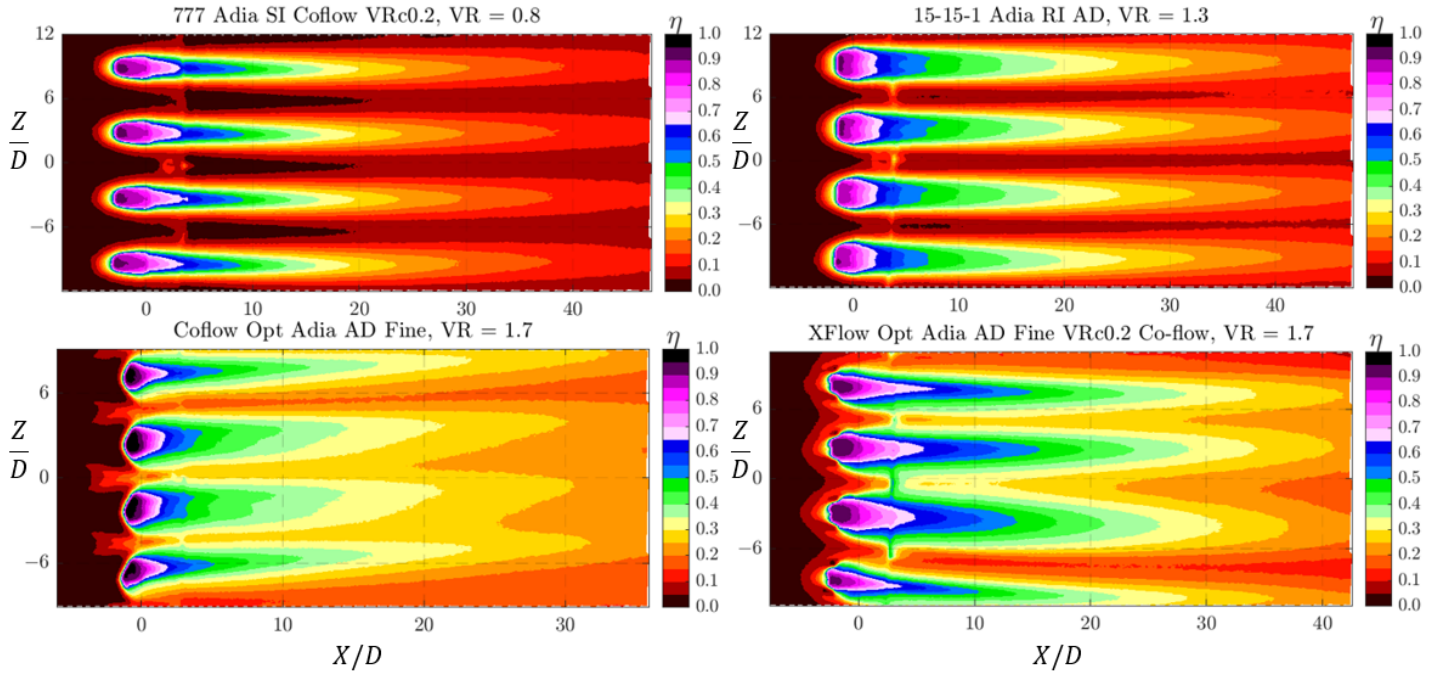

FIGURE 11: ADIABATIC EFFECTIVENESS η CONTOURS AT CORRESPONDING PEAK EFFECTIVENESS *VR*

from the holes were distinctly skewed. A skewness of the flow from the holes might be expected for the X-AOpt holes because the design of the hole is asymmetrical. However, the design of the Co-AOpt hole is symmetrical, so a skewed exit from the hole indicates the coolant flow within the hole has become skewed, likely due to separation within the diffusing section of the hole. As will be discussed in more detail later, the hole to hole variation in coolant hole performance for the Co-AOpt and X-AOpt holes only occurred at higher *VR*s, at lower *VR*s the performance for all holes was very similar.

The η contours shown in Fig. 11 also provide insight on the significantly higher adiabatic effectiveness for the X-AOpt hole compared to the Co-AOpt hole. The η distribution for the Co-AOpt hole is broad and relatively flat in the spanwise direction, whereas the η distribution for the X-AOpt hole has significantly higher η levels at the center of the jet. For example, at *X/D*=10 the Co-AOpt hole has $\eta \approx 0.35$ but the X-AOpt hole has $\eta \approx 0.55$. This much higher centerline value for η for the X-AOpt hole may be attributed to the external protuberances to the sides of the hole generating a strong counter rotating vortex structure that directs coolant towards the wall at the centerline.

The X-AOpt and 15-15-1 RI holes were analyzed in more detail to determine the differences in hole-to-hole area averaged effectiveness. For this analysis, the area averaged adiabatic effectiveness was calculated over the pitch of each of the four holes in measurement range, and over the range *X/D*=5 to 20. Results from this analysis, presented in Fig. 12, quantify the variation of the adiabatic effectiveness performance for each hole in the row of four holes for the X-AOpt and 15-15-1 RI holes. Immediately obvious from this figure is the strong variation in $\bar{\bar{\eta}}$ values for the X-AOpt hole while the 15-15-1 RI hole has essentially no variation among holes. Although the X-AOpt hole had variations in $\bar{\bar{\eta}}$ more than a factor of two for *VR*=3.3, for *VR*=0.4 and 0.8, this hole had negligible variation among holes. Contour plots of η are presented in Fig. 13 for the X-AOpt hole for *VR*=0.8, 1.7, and 3.3. Consistent with Fig. 12, these plots show degradation from uniform performance for all holes at *VR*=0.8, to very non-uniform performance for *VR*=3.3.

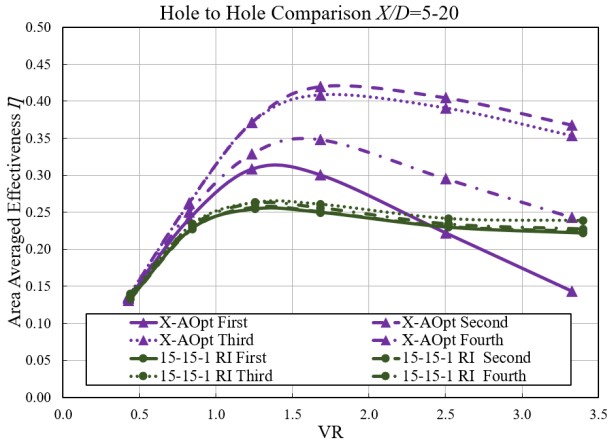

FIGURE 12: AREA AVERAGED ADIABATIC EFFECTIVENESS (HOLE-TO-HOLE COMPARISON, 15-15-1 RI AND X-AOPT)

This change in variability of performance among the holes with increasing *VR* suggests that very small differences in the builds of the holes cause an instability that results in separation in the diffuser section and hence poor performance. If all holes in the row operated optimally, the area averaged adiabatic effectiveness would increase by 10%. Consequently, there is a possibility that further refinement of the X-AOpt hole to obtain more stable

operation would lead to significantly improved performance.

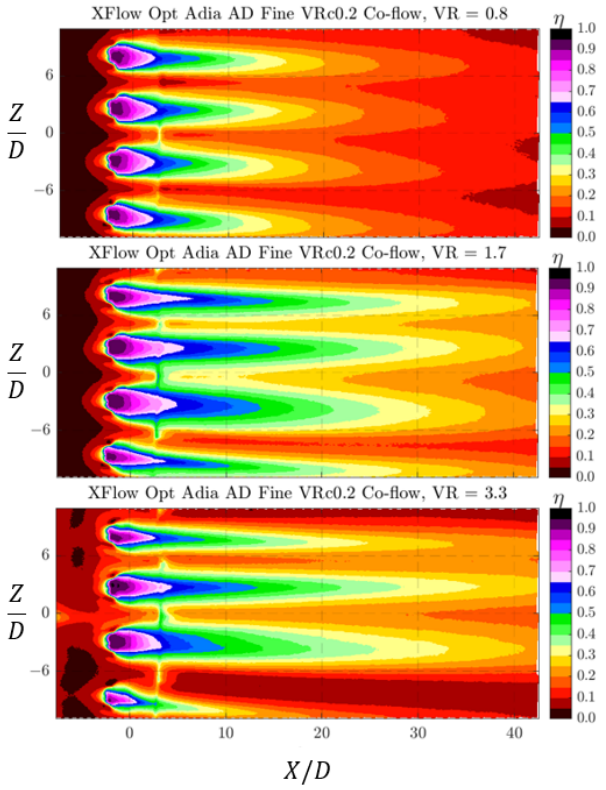

FIGURE 13: ADIABATIC EFFECTIVENESS η CONTOURS FOR THE X-AOPT HOLE WITH VARYING *VR*

3.3 Overall Cooling Effectiveness Results

Overall cooling effectiveness surface measurements for 5X scale holes and 1X scale are presented in this section. Results for 5X matched *Bi* models are presented for X-AOpt and 15-15-1 RI holes. Results for metal 1X scale X-AOpt, Co-AOpt, and 15-15-1 RI geometries are presented in this section. For the analysis of area-averaged overall cooling effectiveness, the area averaged overall effectiveness for the 5X tests was calculated over four hole pitches while for the 1X tests a span of three hole pitches was used. In both cases the streamwise range was *X/D*=5 to 20, which is consistent with the range used for the spatially averaged adiabatic effectiveness.

Area-averaged overall cooling effectiveness, $\bar{\bar{\phi}}$, distributions for the X-AOpt and 15-15-1 RI holes, presented in Fig. 14, show that the two holes have similar performance for *VR*=0.5 and 0.8, but the X-AOpt hole has greater overall cooling effectiveness for higher *VR*s, with as much as 10% greater values at *VR*=1.7. The equivalent $\bar{\bar{\phi}}$ values for the two holes for the lower *VR*s are consistent with the adiabatic effectiveness measurements described earlier. The higher $\bar{\bar{\phi}}$ values for the X-AOpt hole are also consistent with the adiabatic effectiveness results, but the percentage increase was much larger for the adiabatic effectiveness. This difference can be attributed to the overall cooling effectiveness having contributions from internal cooling and bore cooling in the hole beyond the film cooling. The combined internal cooling and bore cooling for these two holes is expected to be similar because of the similar feed and hole size, so the difference in the overall cooling effectiveness for the two holes will be due to differences in the contributions from film cooling effectiveness. Consequently, the overall cooling effectiveness will have a smaller percentage difference than the adiabatic effectiveness.

Also, as discussed previously, the discharge coefficients for the high conductivity (matched *Bi*) X-AOpt model were found to be about 20% lower than the low conductivity (adiabatic) model. This lower discharge coefficient for the high conductivity model suggest that coolant hole was not as efficient in expanding the coolant jet in the diffuser section. This would cause a decrease in cooling performance.

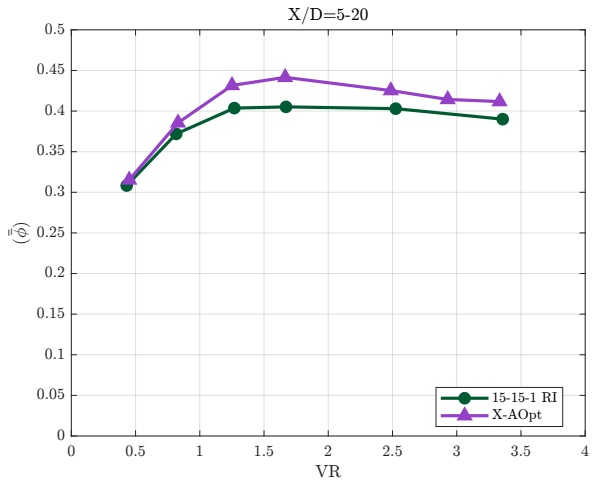

FIGURE 14: COMPARISON OF THE AREA AVERAGED OVERALL COOLING EFFECTIVENESS (*X/D*=5 TO 20) FOR THE X-AOPT AND 15-15-1 RI HOLES

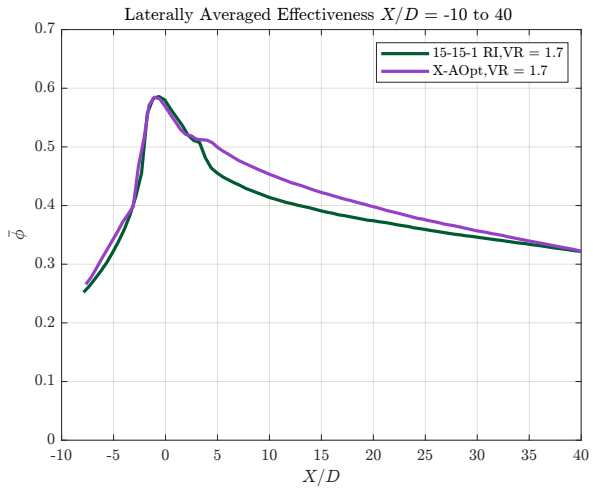

FIGURE 15: LATERALLY AVERAGED OVERALL COOLING EFFECTIVENESS, *VR*=1.7

More insight into overall cooling effectiveness performance for the X-AOpt and the 15-15-1 RI holes are provided by the laterally averaged overall cooling effectiveness distributions, $\bar{\phi}$, and contours of overall cooling effectiveness, ϕ, for *VR*=1.7 which are presented in Figs. 15 and 16, respectively. Distributions of $\bar{\phi}$

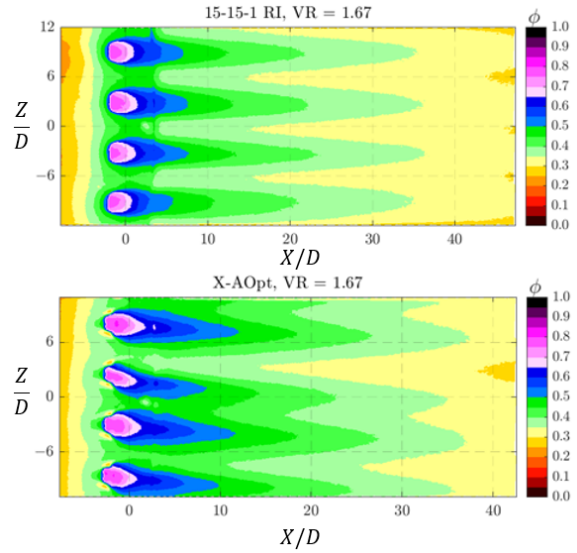

FIGURE 16: OVERALL EFFECTIVENESS ϕ CONTOURS AT CORRESPONDING PEAK EFFECTIVENESS *VR*

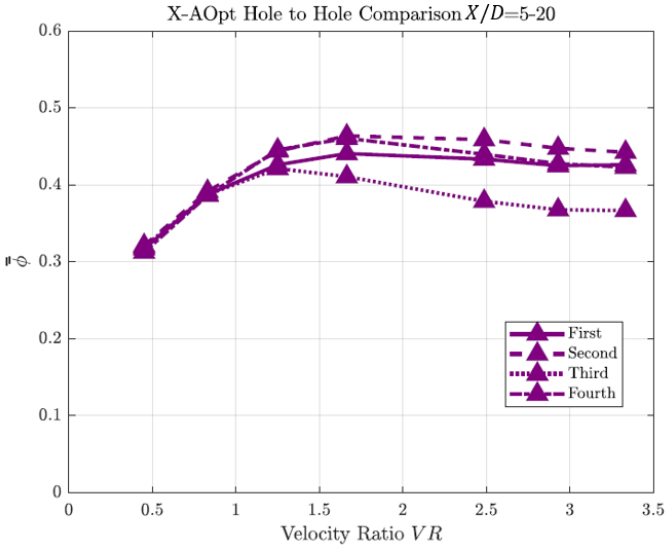

FIGURE 17: AREA AVERAGED OVERALL EFFECTIVENESS (HOLE-TO-HOLE COMPARISON, X-AOPT)

in Fig. 15 show that within and upstream of the hole, the overall cooling effectiveness for the two holes were the same. This is an indication that the bore cooling within the coolant holes were very similar. Downstream of the holes, at *X/D*=5 the $\bar{\phi}$ value for the X-AOpt hole was about 10% higher than that for the 15-15-1 RI hole, but far downstream the of $\bar{\phi}$ values were similar for both holes. These results are consistent with the adiabatic effectiveness results discussed previously. In the associated contour plots of ϕ shown in Fig. 16, the ϕ distribution for the X-AOpt hole is broader and with higher ϕ at the centerline than for the 15-15-1 RI hole, which would account for the higher area averaged overall cooling effectiveness. Also evident in Fig. 16, is that the performance for each of the four 15-15-1 RI holes was very similar, but there were noticeable variations in performance for the four X-AOpt holes. A

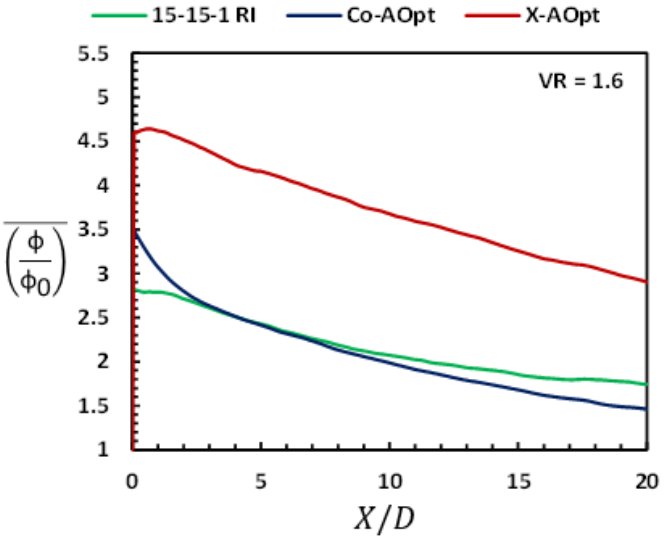

FIGURE 18: LATERAL AVERAGE OF OVERALL EFFECTIVENESS AUGMENTATION LEVELS AT *VR*=1.6 FOR 1X TESTS

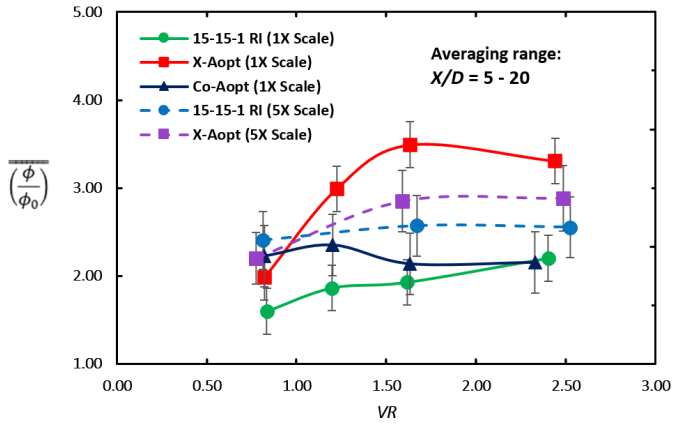

FIGURE 19: AREA-AVERAGED OVERALL EFFECTIVENESS AUGMENTATION FOR THE 1X AND 5X MODEL TESTS

similar variation in performance among holes was found with the adiabatic effectiveness results which was discussed previously. The hole to hole variation for the X-AOpt holes were quantified by determining the area-averaged overall cooling effectiveness for each of the four holes. The hole to hole variations for the $\bar{\bar{\phi}}$ values, presented in Fig. 17, were much less than the variation in $\bar{\bar{\eta}}$ values for the X-AOpt holes discussed previously. This may be attributed to the overall cooling effectiveness having only partial sensitivity to the adiabatic effectiveness since the internal and bore cooling also contribute to the overall cooling effectiveness.

The lateral average of the augmentation in effectiveness for the 15-15-1 RI, the Co-AOpt, and the X-AOpt holes at a *VR*=1.6 are shown in Fig. 18. Fig. 18 clearly shows significantly better cooling performance using the X-AOpt cooling hole relative to the 15-15-1 RI and the Co-AOpt cooling holes along the entire coupon length, which was consistent with the 5X scale results. The $\bar{\phi}/\phi_0$ levels for the Co-AOpt hole and the 15-15-1 RI were

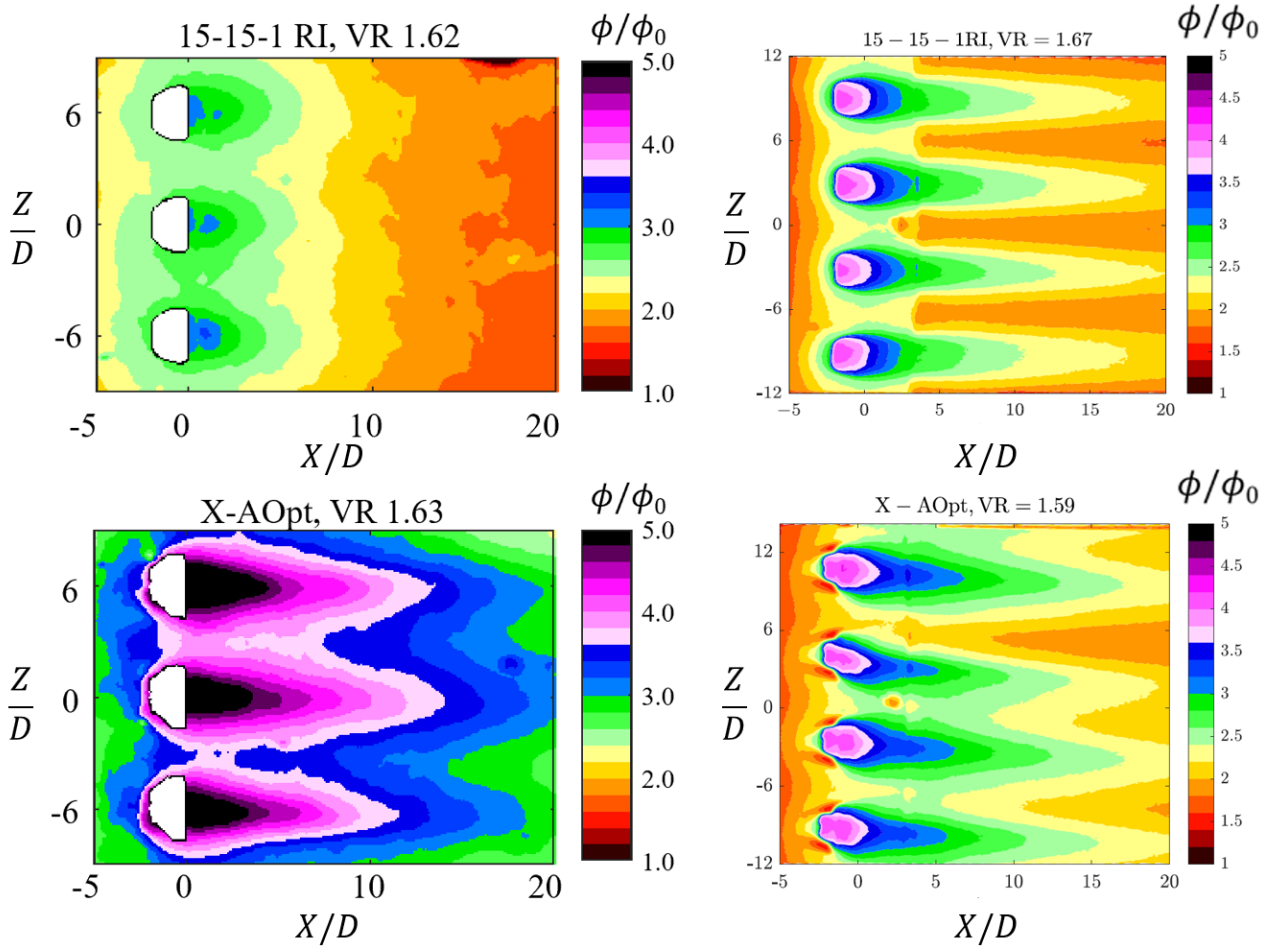

FIGURE 20: OVERALL EFFECTIVENESS AUGMENTATION ϕ/ϕ_0 CONTOURS AT *VR*=1.6 FOR 1X TESTS (LEFT) AND 5X TESTS (RIGHT)

nearly with same with the Co-AOpt showing only slightly better performance near the cooling hole, which may in fact, be a result of the convection within the cooling hole being better for the Co-AOpt hole. The area-average augmentation in overall effectiveness levels, $\bar{\bar{\phi}}/\phi_0$, for the three hole geometries are shown in Fig. 19 over a range of blowing ratios. As was previously discussed, the X-AOpt hole is clearly outperforming the other holes in terms of cooling at velocity ratios beyond *VR*=1.2. The geometry of the X-AOpt resulted in vortices that pushed the coolant towards the surface, which was shown in the CFD during the optimization process [13]. Also shown in Fig. 19, are the area-average augmentation in overall effectiveness levels for the 5X scale X-AOpt and 15-15-1 RI holes. The $\bar{\bar{\phi}}/\phi_0$ values for the 5X scale 15-15-1 RI holes were significantly higher than for the 1X scale model for all *VR*s. However, the $\bar{\bar{\phi}}/\phi_0$ values for the 5X scale X-AOpt holes were similar to that for the 1X scale model at *VR*=0.8, but significantly lower than the 1X scale model at *VR*=1.7.

To gain a better understanding of the area averaged augmented overall effectiveness as presented in Fig. 19, contours of the augmented overall effectiveness $\bar{\bar{\phi}}/\phi_0$ for 1X scale and 5X models at nominally *VR*=1.6 are shown in Fig. 20. As evident by these contours, for the 15-15-1 RI holes, the augmentation factors are similar immediately downstream of the holes, but 5X holes show distinct coolant paths downstream, suggesting less diffusion of the coolant jets. This results in higher cooling effectiveness farther downstream for the 5X holes. On the other hand, the contours for the 1X scale X-AOpt shows much higher augmentation factors immediately downstream of the holes and sustained for a larger distance downstream. Furthermore, the 1X holes show much larger augmentation factors upstream of the film cooling holes, which is an indication that the internal bore cooling for the 1X holes is much larger than for the 5X holes. This increased bore cooling in the holes will raise the augmentation factor upstream and downstream of the holes. The much higher bore cooling for the 1X hole might be attributed to operation at much higher Mach numbers which will result in transonic flows in the film cooling hole. This may greatly enhance turbulence in the hole and hence increased heat transfer rates.

The significant difference between the 1X and 5X models of the X-AOpt holes might be due to the difference in manufacturing. Recall that the 5X models were built close to design intent, while the metal AM build at engine scale had noticeable deviation from the design intent that was shown in Figure 5. A critical reason for the improved performance for the X-AOpt hole is the vortex generating mechanism by the protrusion at the hole exit that generates vortices that appear to bring coolant back to the surface at the centerline of the coolant jet. It is apparent that changes in

these protrusions and the hole exit for the 1X metal AM build, actually improved the vortex generating mechanism and improved performance for this hole. Most importantly, although there were significant differences in the 1X and 5X model tests, there was consistency in finding that maximum overall cooling effectiveness was obtained using the X-AOpt hole.

4. CONCLUSIONS

In this study, the film cooling performance for recently developed film cooling holes designed using adjoint based optimization techniques, X-AOpt and Co-AOpt, were experimentally evaluated including comparisons with two more conventional 15-15-1 RI and 7-7-7 SI holes. Although the X-AOpt hole was designed to provide maximum adiabatic effectiveness when fed from a coolant channel oriented with a 90° cross-stream direction to the mainstream flow, when tested with a co-flowing coolant channel, the X-AOpt hole performed significantly better than Co-AOpt hole which had been designed to provide maximum adiabatic effectiveness with a co-flowing coolant feed channel. Both the X-AOpt and Co-AOpt holes were found to provide significantly greater adiabatic effectiveness than a conventional 7-7-7 SI hole, with the peak area averaged adiabatic effectiveness being 75% greater than the 7-7-7 SI hole. The 15-15-1 RI hole, which was designed from a parametric study of the optimum lateral and forward expansion angles for a laidback fanshaped hole, was found to perform at an intermediate level between the adjoint based optimized holes and the conventional 7-7-7 SI hole. Engine scale metal AM builds of these holes, tested at near engine operating conditions, confirmed the overall cooling effectiveness of the X-AOpt hole was significantly larger than the other hole designs. Measurements of the discharge coefficient for all hole geometries tested showed significantly higher C_d values for X-AOpt hole compared to the other holes. With C_d=1.2 over a wide range of coolant jet velocity ratios, the X-AOpt hole was 50% larger than the conventional 7-7-7 SI hole. This larger C_d value suggests better performance for the diffusing section of the film cooling hole and hence improved film cooling adiabatic and overall cooling effectiveness. Despite the good performance for the X-AOpt hole in terms of area averaged adiabatic effectiveness, significant hole to hole variation in performance was observed. This suggests that flow through these film cooling holes are marginally stable, with some holes not able to achieve good diffusion of the coolant flow through the hole. This suggests the possibility of an improved design in which the coolant flow through each hole is more stable and reliable.

5. ACKNOWLEDGMENTS

The authors would like to thank the U.S. Department of Energy - National Energy Technology Laboratory for sponsoring research presented in this paper. This paper is based upon work supported by the Department of Energy under Award Number DE-FE0031760. This report was prepared as an account of work sponsored by an agency of the United States Government. Neither the United States Government nor any agency thereof, nor any of their employees, makes any warranty, express or implied, or assumes any legal liability or responsibility for the accuracy, completeness, or usefulness of any information, apparatus, product, or process disclosed, or represents that its use would not infringe privately owned rights. Reference herein to any specific commercial product, process, or service by trade name, trademark, manufacturer, or otherwise does not necessarily constitute or imply its endorsement, recommendation, or favoring by the United States Government or any agency thereof. The views and opinions of authors expressed herein do not necessarily state or reflect those of the United States Government or any agency thereof.

REFERENCES

[1] Schurb, Julius, Hoebel, Matthias, Haehnle, Hartmut, Kissel, Harald, Bogdanic, Laura and Etter, Thomas. "Additive Manufacturing of Hot Gas Path Parts and Engine Validation in a Heavy Duty GT." *Volume 6: Ceramics; Controls, Diagnostics and Instrumentation; Education; Manufacturing Materials and Metallurgy*: p. V006T21A005. 2016. American Society of Mechanical Engineers, Seoul, South Korea. DOI 10.1115/GT2016-57262. Accessed 2021-12-19, URL https://asmedigitalcollection.asme.org/GT/proceedings/GT2016/49828/Seoul,%20South%20Korea/240582.

[2] Min, Zheng, Huang, Gan, Parbat, Sarwesh Narayan, Yang, Li and Chyu, Minking K. "Experimental Investigation on Additively Manufactured Transpiration and Film Cooling Structures." *Journal of Turbomachinery* Vol. 141 No. 3 (2019): p. 031009. DOI 10.1115/1.4042009. Accessed 2021-12-19, URL https://asmedigitalcollection.asme.org/turbomachinery/article/doi/10.1115/1.4042009/475729/Experimental-Investigation-on-Additively.

[3] Stimpson, Curtis K., Snyder, Jacob C., Thole, Karen A. and Mongillo, Dominic. "Effectiveness Measurements of Additively Manufactured Film Cooling Holes." *Journal of Turbomachinery* Vol. 140 No. 1 (2018): p. 011009. DOI 10.1115/1.4038182. Accessed 2020-11-12, URL https://asmedigitalcollection.asme.org/turbomachinery/article/doi/10.1115/1.4038182/421677/Effectiveness-Measurements-of-Additively.

[4] Snyder, Jacob C. and Thole, Karen A. "Effect of Additive Manufacturing Process Parameters on Turbine Cooling." *Journal of Turbomachinery* Vol. 142 No. 5 (2020): p. 051007. DOI 10.1115/1.4046459. Accessed 2020-11-12, URL https://asmedigitalcollection.asme.org/turbomachinery/article/doi/10.1115/1.4046459/1074872/Effect-of-Additive-Manufacturing-Process.

[5] Snyder, Jacob C. and Thole, Karen A. "Performance of Public Film Cooling Geometries Produced Through Additive Manufacturing." *Journal of Turbomachinery* Vol. 142 No. 5 (2020): p. 051009. DOI 10.1115/1.4046488. Accessed 2021-12-19, URL https://asmedigitalcollection.asme.org/turbomachinery/article/142/5/051009/1074954/Performance-of-Public-Film-Cooling-Geometries.

[6] Fraas, Marc, Glasenapp, Tobias, Schulz, Achmed and Bauer, Hans-Jörg. "Optimized inlet geometry of a laidback fan-shaped film cooling hole–Experimental study of film cooling performance." *International Journal of Heat and Mass Transfer* Vol. 128 (2019): pp. 980–990.

[7] Jones, Fraser B., Fox, Dale W. and Bogard, David G. "Experimental and Computational Investigation of Shaped Film Cooling Holes Designed to Minimize Inlet Separation." 2020. American Society of Mechanical Engineers, London, England.

[8] Jones, Fraser B., Fox, Dale W., Oliver, Todd and Bogard, David G. "Parametric Optimization of Film Cooling Hole Geometry." *Volume 5A: Heat Transfer — Combustors; Film Cooling*: p. V05AT12A013. 2021. American Society of Mechanical Engineers, Virtual, Online. DOI 10.1115/GT2021-59326. Accessed 2021-12-15, URL https://asmedigitalcollection.asme.org/GT/proceedings/GT2021/84973/V05AT12A013/1120039.

[9] Dyson, Thomas E., McClintic, John W., Bogard, David G. and Bradshaw, Sean D. "Adiabatic and Overall Effectiveness for a Fully Cooled Turbine Vane." *Volume 3B: Heat Transfer*: p. V03BT13A037. 2013. American Society of Mechanical Engineers, San Antonio, Texas, USA. DOI 10.1115/GT2013-94928. Accessed 2021-03-10, URL https://asmedigitalcollection.asme.org/GT/proceedings/GT2013/55157/San%20Antonio,%20Texas,%20USA/249700.

[10] Anderson, Joshua B., Boyd, Emily J. and Bogard, David G. "Experimental Investigation of Coolant-to-Mainstream Scaling Parameters With Cylindrical and Shaped Film Cooling Holes." *Volume 5B: Heat Transfer*: p. V05BT12A033. 2015. American Society of Mechanical Engineers, Montreal, Quebec, Canada. DOI 10.1115/GT2015-43072. Accessed 2021-12-19, URL https://asmedigitalcollection.asme.org/GT/proceedings/GT2015/56727/Montreal,%20Quebec,%20Canada/237488.

[11] Yoon, Christopher, Gutierrez, Daniel, Furgeson, Michael T. and Bogard, David G. "Evaluation of Adjoint Optimized Hole - Part II: Parameter Effects on Performance." *Proceedings of ASME Turbo Expo 2022*. 2022. American Society of Mechanical Engineers, Rotterdam, The Netherlands. DOI GT2022-82726.

[12] Veley, Emma M., Furgeson, Michael T., Thole, Karen A. and Bogard, David G. "Printability and Overall Cooling Performance of Additively Manufacturing Holes With Inlet and Exit Rounding." *Proceedings of ASME Turbo Expo 2022*. 2022. American Society of Mechanical Engineers, Rotterdam, The Netherlands. DOI GT2022-83313.

[13] Jones, Fraser B., Oliver, Todd and Bogard, David G. "Adjoint Optimization of Film Cooling Hole Geometry." *Volume 5A: Heat Transfer — Combustors; Film Cooling*: p. V05AT12A014. 2021. American Society of Mechanical Engineers, Virtual, Online. DOI 10.1115/GT2021-59332. Accessed 2021-12-15, URL https://asmedigitalcollection.asme.org/GT/proceedings/GT2021/84973/V05AT12A014/1120028.

[14] Furgeson, Michael T., Veley, Emma M., Yoon, Christopher, Gutierrez, Daniel, Bogard, David G. and Thole, Karen A. "Development and Evaluation of Shaped Film Cooling Holes Designed for Additive Manufacturing." *Proceedings of ASME Turbo Expo 2022*. 2022. American Society of Mechanical Engineers, Rotterdam, The Netherlands. DOI GT2022-83201.

[15] Fox, Dale W., Jones, Fraser B., McClintic, John W., Bogard, David G., Dyson, Thomas E. and Webster, Zachary D. "Rib Turbulator Effects on Crossflow-Fed Shaped Film Cooling Holes." *Journal of Turbomachinery* Vol. 141 No. 3 (2019): p. 031013. DOI 10.1115/1.4041673. Accessed 2019-12-11, URL https://asmedigitalcollection.asme.org/turbomachinery/article/doi/10.1115/1.4041673/475791/Rib-Turbulator-Effects-on-CrossflowFed-Shaped-Film.

[16] Moffat, Robert J. "Describing the uncertainties in experimental results." *Experimental Thermal and Fluid Science* Vol. 1 No. 1 (1988): pp. 3–17. DOI 10.1016/0894-1777(88)90043-X. Accessed 2019-12-11, URL https://linkinghub.elsevier.com/retrieve/pii/089417778890043X.

[17] Gritsch, M., Saumweber, C., Schulz, A., Wittig, S. and Sharp, E. "Effect of Internal Coolant Crossflow Orientation on the Discharge Coefficient of Shaped Film-Cooling Holes." *Journal of Turbomachinery* Vol. 122 No. 1 (2000): pp. 146–152. DOI 10.1115/1.555436. Accessed 2020-05-28, URL https://asmedigitalcollection.asme.org/turbomachinery/article/122/1/146/419806/Effect-of-Internal-Coolant-Crossflow-Orientation.

[18] Gritsch, M., Schulz, A. and Wittig, S. "Discharge Coefficient Measurements of Film-Cooling Holes With Expanded Exits." *Volume 3: Heat Transfer; Electric Power; Industrial and Cogeneration*: p. V003T09A030. 1997. American Society of Mechanical Engineers, Orlando, Florida, USA. DOI 10.1115/97-GT-165. Accessed 2019-12-11, URL https://asmedigitalcollection.asme.org/GT/proceedings/GT1997/78705/Orlando,%20Florida,%20USA/237967.

[19] Gritsch, Michael, Colban, Will, Schär, Heinz and Döbbeling, Klaus. "Effect of Hole Geometry on the Thermal Performance of Fan-Shaped Film Cooling Holes." *Journal of Turbomachinery* Vol. 127 No. 4 (2005): pp. 718–725. DOI 10.1115/1.2019315. Accessed 2022-04-11, URL https://asmedigitalcollection.asme.org/turbomachinery/article/127/4/718/464205/Effect-of-Hole-Geometry-on-the-Thermal-Performance.